Int. j. adv. multidisc. res. stud. 2023; 3(2):1162-1166

Received: 08-03-2023
Accepted: 18-04-2023

International Journal of Advanced Multidisciplinary Research and Studies

ISSN: 2583-049X

Physical and Magnetic Behaviour of Mn^{4+} Substitution on Ni-Mn Ferrite

[1] JS Lad, [2] CM Kale

[1] Department of Physics, Government Arts, and Science College, Aurangabad, Maharashtra, India
[2] Department of Physics, Indraraj Arts, Commerce, and Science College, Sillod-Aurangabad, Maharashtra, India

Corresponding Author: **CM Kale**

Abstract
The ultrafine ferrite material having general formula $Ni_{1+x}Mn_xFe_{2-2x}O_4$; where $0.0 \leq x \leq 0.6$ were prepared through double sintering solid state reaction technique using A.R. grade oxides of respective ions. The phase purity of all the samples was checked by X-ray diffraction technique. The X-ray diffraction pattern shows all reflections belonging to cubic spinel structure. No extra peak other than cubic spinel was observed in the X-ray diffraction pattern. Using X-ray diffraction pattern data and using Braggs law, the lattice constant was calculated for all the compositions. The lattice constant decreases linearly with Mn^{4+} substitutions and obeys Vegard's law. The magnetic properties (saturation magnetization, magneton number, coercivity etc.) were investigated using pulse field hysteresis loop technique at room temperature. The values of coercivity decreases with Mn^{4+} content increases. The saturation magnetization and magneton number both significantly decreases with increase in Mn^{4+} substitution.

Keywords: Spinel Ferrite, X-Ray Diffraction, Lattice Constant, Magneton Number, Coercivity

1. Introduction

Now a days the researcher was attracted by magnetic materials. Ferrite is a good magnetic material, which are magnetic oxides, form a class of very good magnetic material because of their high electrical resistivity, low eddy current and dielectric losses, high saturation magnetization, high Curie temperature and high permeability [1]. These important properties of ferrites are the basis of its technological importance in many fields. These remarkable properties of ferrites are useful in many applications such as transformer core, antenna rods, memory chips, magnetic sensors, drug delivery etc. [2]. The important magnetic and electrical properties of ferrites mainly depend on methods of preparation, type and amount of dopant, cation distribution etc. [3].

On the basis of crystal structure, ferrites are grouped into three important classes, namely spinel ferrite, garnet and hexa-ferrite [4]. Spinel ferrites are represented by the formula AFe_2O_4, where A is a divalent metal ion. The crystal structure of ferrite consists of two interstitial sites, tetrahedral (A) and octahedral [B] sites; in which cations are occupied. The magnetic properties are linked with the A-B magnetic interaction between the magnetic atoms on the tetrahedral (A) and octahedral [B] sites. Thus, it is essential to know the distribution of cations over available tetrahedral (A) and octahedral [B] sites in order to understand magnetic properties of spinel ferrites. The cation distribution in spinel ferrites can be studied by using X-ray diffraction method [5], magnetization [6], Mossbauer [7] and neutron diffraction technique [8]. Among the spinel ferrites, nickel ferrite is a typical inverse spinel ferrite and is extensively used in many applications because of its large permeability at high frequency, remarkable high electrical resistivity, moderate saturation magnetization, Curie temperature, chemical stability and cost effectiveness [9]. Nickel and substituted nickel ferrites have been studied for their various properties by many researchers [10-11]. The effect of divalent and trivalent ions on the structural, electrical and magnetic properties of nickel ferrite has been reported in literature [12, 13]. In the literature, effect of tetravalent substitution of Mn4+ ions on the properties of nickel ferrite have been reported by very few workers [14]. However, cation distribution and their correlation with magnetic properties have not been reported in the literature. Mn^{4+} is a non-magnetic ion, when two Fe^{3+} ions are replaced by Mn^{4+} ions in combination with divalent Ni^{2+} ions, may result in improved magnetic and electrical properties of nickel ferrite. To our knowledge, the structural and magnetic properties of Mn^{4+} substituted nickel ferrite has not been investigated in detail and correlated with the cation distribution.

In this research article, attempt has been made to synthesize nickel ferrite with Mn^{4+} substitution with the chemical formula $Ni_{1+x}Ti_xFe_{2-2x}O_4$; where $0.0 \leq x \leq 0.7$. The physical and magnetic properties were investigated by means of X-ray diffractometry, magnetization spectral studies.

2. Experimental

The polycrystalline samples of $Ni_{1+x}Ti_xFe_{2-2x}O_4$, where $0.0 \leq x \leq 0.7$, in the step of 0.1were prepared by double sintering ceramic technique [15]. The A.R. grade oxides (SD Fine) of corresponding ions (NiO, TiO_2 and Fe_2O_3) were mixed in stoichiometric proportions. Each sample was wet ground for 4 hours using agate mortar. The samples were pre-sintered in a muffle furnace at 900ºC for 12 hours. The pre-sintered samples were reground and compressed into a pellet form using hydraulic press with a pressure of 6 ton per inch^2. These pellets were sintered at 1200ºC in air for 24 hours and were slowly cooled to room temperature. X-ray diffraction (XRD) patterns were recorded at room temperature in the 2θ range of 20^0 to 80^0 to confirm the single-phase cubic spinel structure. The cation distribution was estimated through X-ray diffraction technique. The magnetic properties were studied using pulse field hysteresis loop technique at room temperature [16].

3. Results and discussion

3.1 Structural properties

Room temperature X-ray diffraction patterns of typical samples 0.1, 0.2 and 0.3 the samples of the series $Ni_{1+x}Mn_x Fe_{2-2x}O_4$; where $x = 0.0 \leq x \leq 0.6$, are shown in Fig 1. XRD analysis showed that the samples under investigation have cubic spinel structure; no extra peak has been observed other than the cubic spinel. All the peaks are found to be sharp and intense.

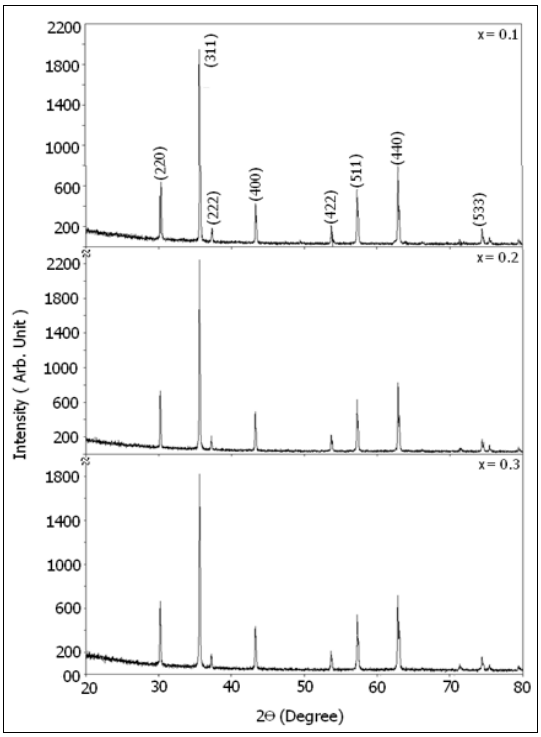

Fig 1: X-ray diffraction patterns of typical samples of $Ni_{1+x}Mn_x Fe_{2-2x}O_4$; where x = 0.1, 0.2 and 0.3

The values of Miller indices (hkl), Bragg's angle (2θ), inter planer spacing (d) and peak intensity for each Bragg's peak**.** It can be observed that the inter planer spacing value (d) changes with the addition of Mn content x. The XRD data was used to calculate the lattice constant of all samples. The values of lattice constant obtained from XRD data with an accuracy of ± 0.002 are given in Table 1.

The variation of lattice constant with Mn content x is observed from Table 1, that the lattice constant of $Ni_{1+x}Mn_xFe_{2-2x}O_4$ increases from x = 0.0 to x = 0.1, beyond x = 0.1 the lattice constant decreases with Mn content x. The decrease in lattice constant with Mn content x is attributed to the difference in ionic radii of constituent ions i.e., Ni^{2+}, Fe^{3+} and Mn^{4+}. In the present series $Ni_{1+x}Mn_xFe_{2-2x}O_4$ two Fe^{3+} (0.67Å) ions are replaced by combination of Ni^{2++}(0.72Å) ions and Mn^{4+}(0.52Å), thereby decreasing the lattice constant of the system should decrease. A similar result of variation of lattice constant in tetrahedral substitution is observed [17]. The decrease in lattice constant is almost linear and obeys Vegards law [18].

Table 1: Values of Lattice constant (a), Particle size, X-Ray density and % Porosity of $Ni_{1+x}Mn_x Fe_{2-2x}O_4$; where $x = 0.0 \leq x \leq 0.6$ system

Mn content x	**Lattice constant** (Å)	**X-Ray density** (gm/cm^3)	**Particle Size** (Å)
0.0	8.337	6.781	499
0.1	8.362	6.452	454
0.2	8.355	6.198	555
0.3	8.349	5.942	454
0.4	8.336	5.696	501
0.5	8.327	5.443	499
0.6	8.323	5.179	416

The X-ray density (dx) was calculated for all the values of x and the values are presented in Table 1. Table 1, indicates that X-ray density decreases linearly with Mn content x. The decrease in X-ray density is attributed to the fact that decrease in mass over take the decrease in volume of the unit cell. Similar behaviors of X-ray density were also reported in the literature [19].

The particle size of each sample was determined by considering most intense peak (311) of the XRD pattern. The particle size was determined by using Scherrer formula,

$$t = \frac{0.9\,\lambda}{\beta \cos\theta}$$

The values of particle size of each sample were reported in the Table 1.

3.2 Cation distribution

The study of cation distribution in spinel ferrite is important to understand the magnetic behaviour of the samples. X-ray diffraction [20] Neutron diffraction [21] and Mössbauer [22] are the techniques available to determine the cation distribution in a given spinel ferrite. In the present work X-ray diffraction method has been used to study the cation distribution. In X-ray diffraction method, X-ray intensity ratios of a selected plane were calculated and the calculated intensity is then compared with the observed intensity ratios. The intensity ratios were calculated for various distributions of cations at tetrahedral (A) and octahedral [B] sites. An agreement factor given by,

$$R = \left| \frac{I^{obs}_{hkl}}{I^{obs}_{h'k'l'}} - \frac{I^{cal.}_{hkl}}{I^{cal.}_{h'k'l}} \right|$$

The minimum value of R gives the best possible cation distribution. The intensity 'I' of given diffraction line can be

calculated using following relation.

$$I_{hkl} = | F_{hkl} |^2 P L_P$$

Where, F_{hkl} is structure factor, P is multiplicity factor, and $L_P$is Lorentz polarization factor.

$$L_p = \frac{1+\cos^2\theta}{\sin^2\theta \cdot \cos 2\theta}$$

The structure factor, multiplicity factor and Lorentz polarization factor are taken from the literature [23]. In the present work (400), (422), (440) planes were considered to calculate intensity ratio. These planes are assumed to be sensitive to the cation distribution. The temperature and absorption factors are not taken into account in our calculations as they do not affect the intensity calculations.
The cation distributions calculated from X-ray intensity ratio calculation is illustrated in Table 2. The table shows that Ni^{2+} occupies octahedral (B) and tetrahedral [B] sites where as Mn^{4+} and Fe^{3+} both occupy tetrahedral (A) and octahedral [B] sites.
The mean ionic radius of the tetrahedral (A) and octahedral [B] sites (r_A and r_B) can be calculated by the following relations.

$$r_A = [1- (x-y) r Fe^{3+} + (x-y) r Mn^{4+}] \text{ and}$$
$$r_B = [1- (x-y) r Fe^{3+} + yr Mn^{4+} + (x-y) r Ni]$$

Where, y is concentration of Mn^{4+} in octahedral [B] site. The values of r_A and r_B with average value of 'r' are given in Table 2. It is clear that both r_A and r_B is decreases with decrease in Mn content x. The decrease in r_A and r_B is due to the replacement of Fe^{3+} ions (0.67Å) by smaller Mn^{4+} (0.52Å) at both sites.

Table 2: Site preference of cations in ferrite and ionic radii 'r_A', 'r_B', average ionic radii of $Ni_{1+x}Mn_x Fe_{2-2x}O_4$; where x = 0.0 ≤ x ≤ 0.6 system

	Site	Type of cations			$R=\frac{Fe^{3+}[B]}{Fe^{3+}(A)}$	r_A (Å)	r_B (Å)	Average r (Å)
		Ni^{2+}	Mn^{4+}	Fe^{3+}				
0.0	A	0.0	0.00	1.00	1.000	0.640	0.690	0.665
	B	1.0	0.00	1.00				
0.1	A	0.0	0.07	0.93	0.935	0.636	0.695	0.666
	B	1.1	0.03	0.87				
0.2	A	0.0	0.14	0.86	0.860	0.632	0.700	0.666
	B	1.2	0.06	0.74				
0.3	A	0.0	0.18	0.82	0.707	0.628	0.705	0.667
	B	1.3	0.12	0.58				
0.4	A	0.0	0.24	0.76	0.579	0.624	0.710	0.667
	B	1.4	0.16	0.44				
0.5	A	0.0	0.30	0.70	0.429	0.620	0.715	0.668
	B	1.5	0.20	0.30				
0.6	A	0.0	0.36	0.64	0.250	0.616	0.720	0.668
	B	1.6	0.24	0.16				

3.3 Infrared spectra

The infrared spectra of all the sample of the ferrite system $Ni_{1+x}Mn_xFe_{2-2x}O_4$ were taken at room temperature in the region 200 cm^{-1} to 800 cm^{-1}. IR spectra of typical sample (x=0.3) are shown in Fig 2.

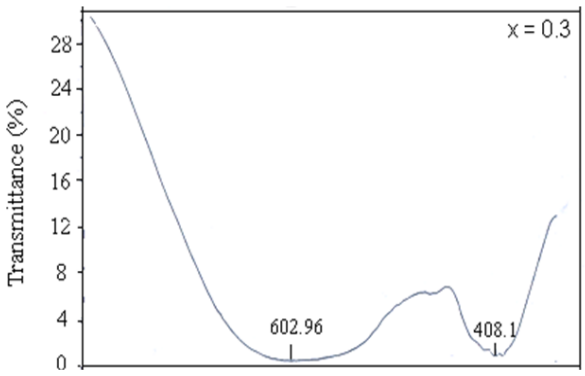

Fig 2: IR spectra of typical sample (x=0.3) for $Ni_{1+x}Mn_x Fe_{2-2x}O_4$; where x = 0.0 ≤ x ≤ 0.6 system

Table 3: Values of vibration band frequencies 'ν_1' and 'ν_2' with force constant 'K_t' and 'K_o' of$Ni_{1+x}Mn_x Fe_{2-2x}O_4$; where x=0.0, 0.3 and 0.5 system

Mn content x	ν_1 cm^{-1}	ν_2 cm^{-1}	$K_t \times 10^5$ dynes/cm	$K_o \times 10^5$ dynes/cm
0.1	605.34	408.9	1.557	1.019
0.3	602.96	408.1	1.539	1.020
0.5	608.41	413.56	1.561	1.052

The spectra show two prominent absorption bands near 400cm^{-1} and 600cm^{-1}. The high frequency band υ_1(600$cm^{-1}$and low frequency band υ_2 (400cm^{-1}) is assigned to intrinsic vibrations of tetrahedral and octahedral groups respectively. The position of two absorption IR bands υ_1 and υ_2 is listed in Table 3. The difference in band position for the various compositions was expected because of the difference in the distance for the octahedral [B] site and tetrahedral (A) site ion.
A similar IR spectrum has been reported by various workers [24, 25]. The IR data have been used to evaluate force constant K_t and K_o for tetrahedral (A) and octahedral [B] sites respectively by using the following relation:

$$K_t = 7.62 \times M_1 \times \upsilon_1^2 \times 10^{-3}$$
$$K_0 = 5.31 \times M_2 \times \upsilon_2^2 \times 10^{-3}$$

Where, υ_1 is high frequency band and υ_2 low frequency band he values of force constant K_t and K_0 are listed in Table 3.

3.4 Magnetic properties

The magnetic hysteresis curve of $Ni_{1+x}Mn_xFe_{2-2x}O_4$ for typical sample x=0.4 and x=0.5 as shown in Fig 3. It can be seen that all the samples show ferrimagnetic behavior which decreases with increase in Mn content x. These hysteresis curves are used to determine, saturation magnetization (M_s), magneton number (n_B), coercivity (H_c) and remanence field (M_r).

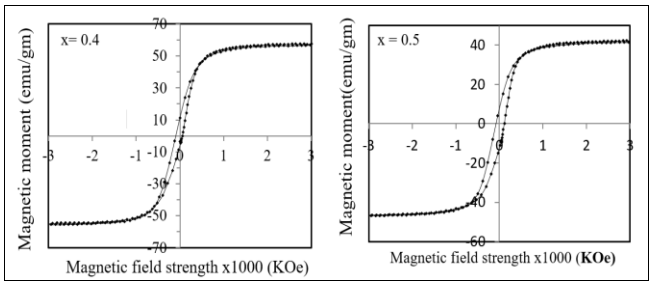

Fig 3: The magnetic hysteresis curve of $Ni_{1+x}Mn_xFe_{2-2x}O_4$ for typical sample x=0.4 and x=0.5

The values of all these magnetic parameters are presented in Table 4. It can be observed from Table 4 that saturation magnetization (M_s) increases with Mn content x up to x = 0.3. After x = 0.3 Ms decreases with Mn content x. The observed behavior of saturation magnetization is similar to that of another well-known spinel ferrite [26]. The observed behaviour of magneton number (n_B) is tried to explain on the basis of Neel's two sub-lattice collinear spin model. According to Neel's two sub-lattice collinear spin model magneton number 'n_B' is given by,

$$n_B = |M_B - M_A|$$

According to Neel's theory n_B is the difference between magnetic moments of ions on A- site and B-site, Where M_A and M_B are the A and B sub lattice magnetic moment in μ_B. The calculated values of magneton number are given in Table 4.

Table 4: Values of magnetic moment of tetrahedral A-site and octahedral B-site and observed and calculated magneton number (μB) $Ni_{1+x}Mn_xFe_{2-2x}O_4$ ($x=0.0 \le x \le 0.6$) system

Mn content x	Magnetic moment (μ_B)		Magneton number 'n_B' (μ_B)	
	M_A	M_B	Obs.	Cal.
0.0	5.0	7.0	1.82	2.0
0.1	4.8	6.7	2.08	1.9
0.2	4.6	6.4	2.25	1.8
0.3	4.4	6.1	2.30	1.7
0.4	4.2	5.8	1.72	1.6
0.5	4.0	5.5	1.15	1.5
0.6	3.8	5.2	0.82	1.4

It is seen from Table 4 that Neel's magneton number decreases with increase in Mn content x. The calculated values of magneton number are given in Table 4. It can be seen from Table 4 that there is a discrepancy in the observed and calculated values of magneton number for x > 0.2. Thus, Neel's theory fails to explain observed behavior of magneton number [27].

4. Conclusions

The experimental results on structural and magnetic properties of Mn^{4+} substituted nickel ferrite system leads us to draw the following conclusions:

1. The prepared samples of $Ni_{1+x}Ti_xFe_{2-2x}O_4$ ($0.0 \le x \le 0.7$) are single phase in nature with cubic spinel structure.
2. The lattice constant decreases with Mn^{4+} substitution.
3. The cation distributions shows that Ni^{2+} occupies octahedral (B) and tetrahedral [B] sites where as Mn^{4+} and Fe^{3+} both occupy tetrahedral (A) and octahedral [B] sites.
4. Both ionic radii r_A and r_B is decreases with decrease in Mn content x. The decrease in r_A and r_B is due to the replacement of Fe^{3+} ions (0.67Å) by smaller Mn^{4+} (0.52Å) at both sites.
5. Saturation magnetization (M_s) increases with Mn content x up to x = 0.3. After x = 0.3 Ms decreases with Mn content x and also magneton number, both decrease with Mn^{4+} substitution.

5. References

1. Kawade VB, Bichile GK, Jadhav KM. Matter. Lett. 2000; 42(33).
2. Vinod N, Dhage ML, Mane MK, Babrekar CM, Kale KM, Jadhav J. Alloys Compd. 2009; 479:863.
3. John Berchmans L, Kali Selvan R, Selva Kumar PN, Magn J. Magn. Mater. 2004; 279:103.
4. Rodrigue GP, IEE Trans, Micro. Theory Tech. 1969; 11:351.
5. Al-Rawas AD, Rais R, Yousif AA, Gismelseed AM, Elzain ME, Mazen S, Al- Falaky A, Magn J. Magn. Mater. 2004; 269:168-175.
6. Alvarez G, Montiel H, Barron JF, Gutierrez MP, Zamorano R, Magn J. Magn. Mater. 2010; 322:248-352.
7. Sharma RK, Suwalka O, Lakshmi N, Venugopalan Hyp K. Interact. 2005; 165:261-266.
8. Corliss LM, Hastings JM. Physical Review. 1953; 90:1013-1018.
9. Costa ACFM, Lula RT, Kiminami RHGA, Gama LFV, De Jusus AD, Andrade HMC. Mater J. Sci. 41, 4871-7875.
10. Chinnasamy CN, Narayansamy S, Panandian N, Justin Joseyphus R, Jeyadevan B, Tohji K, *et al*. Magn J. Magn. Mater. 2002; 238:281-287.
11. Prem Chand, Ramesh C, Srivastava, Anuj Upadhyay J. Alloy Compunds. 2008; 460:108-114.
12. Thummer KP, Chhantbar MC, Modi KB, Baldha GJ, Joshi HH. Mater. Lett. 58, 2248- 2251.
13. Trivedi UN, Modi KB, Joshi HH. Pramana. 2002; 58:1031.
14. Ahmed MA, Abd-Ellatif G, Rashad M. Magn J. Magn. Mater. 2001; 232:194-204.
15. Shinde SS, Jadhav KM, Bichile GK, Bimal S, Trivedi Kulkarni RG. Bull.Mater. Sci. 1998; 21:409-413.
16. Date SK, Joy PA, Anilkumar PS, Shahoo B, Keune W. Phys. Stat. Sol. (c). 2004; 1(12):495-3498.
17. Thummer KP, Chantbar MC, Modi KB, Joshi HH. Indian J. Phys. 2005; 79(1):41-45.
18. Misbah-ul-Islam, Hashmi KA, Rana MU, Abbas T. Solid. State Comm. 2002; 121:51-54.
19. Cullity BD. Elements of X-ray diffraction. Addision-Wessley Publishing Company Ltd, 1959.
20. Burger MJ. Crystal Structure analysis. John Wiley, New York, 1960.
21. Ping Hu, Hai-bo yang, De-an Pan, Hua Wang, Jian-jun Tian, Shen-gen Zhang, Xin-feng, Wang, Alex A. Volinsky J. Magn. Magn. Mater. 2010; 322:173-177.
22. Mathew George, Asha Mary John, Swapna S, Nair PA, Joy MR, Ananthraman J. Magn. Magn. Mater. 2006; 302:190-195.
23. Qiang-Min Wei, Jian-bao Li, Yong-jun Chen, Yong-sheng Han. Mater. Chem. Phys. 2002; 74:340-343.
24. Shinde SS, Jadhav KM. Mater J. Sci. 1998; 17:849-851.
25. Jalaly M, Enayati MH, Kameli P, Karimzadeh F.

Physica B. 2010; 405:507-512.
26. Mundada O, Kunal B, Modi KM, Jadhav GK, Bichile, Ind. J. Pure and Appl. Phys. 1997; 35:554.
27. Amer MA, El Hiti M, Magn J. Magn. Mater. 2001; 234:118-125.